Resource

Cell Reports

Concordant but Varied Phenotypes among Duchenne Muscular Dystrophy Patient-Specific Myoblasts Derived using a Human iPSC-Based Model

Graphical Abstract

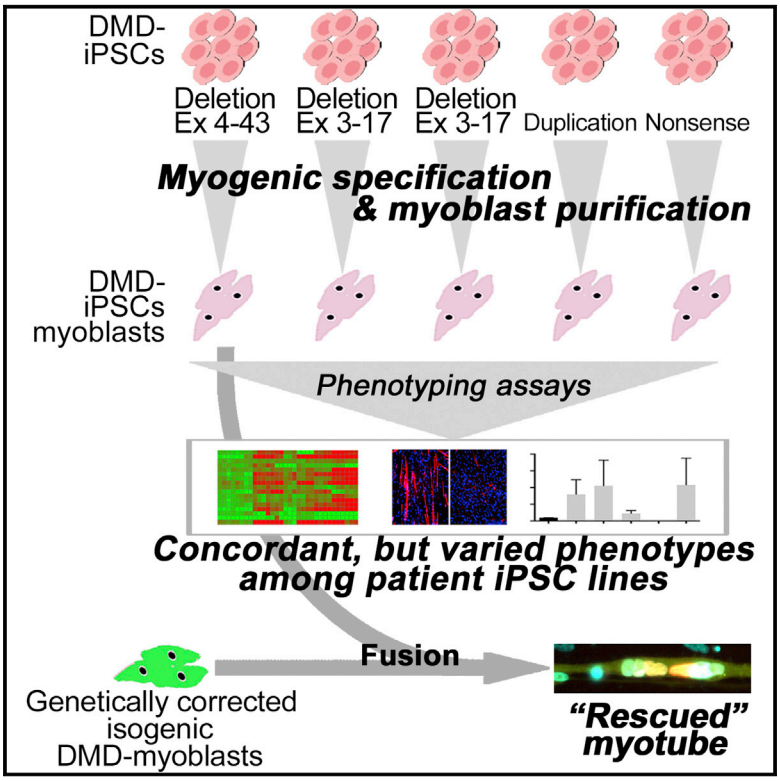

Highlights

- Isolation of functional myoblasts from multiple hiPSC lines using a defined system
- Concordant but heterogeneous phenotypes among myoblasts from DMD patients
- Genetic and pharmacological rescue of DMD-related phenotypes
- Myotube formation in DMD-myoblasts and genetically corrected isogenic myoblasts

Authors

In Young Choi, HoTae Lim, Kenneth Estrellas, ..., Nicholas Maragakis, Kathryn R. Wagner, Gabsang Lee

Correspondence

wagnerk@kennedykrieger.org (K.R.W.), glee48@jhmi.edu (G.L.)

In Brief

Choi et al. show that human iPSC (hiPSC)-derived myoblasts from Duchenne muscular dystrophy patients have aberrant phenotypes with patient-to-patient variability. The cells can be partially rescued by either genetic correction or chemical compound treatments.

Accession Numbers

GSE70955

Choi et al., 2016, Cell Reports *15*, 2301–2312
June 7, 2016
http://dx.doi.org/10.1016/j.celrep.2016.05.016

Cell Reports
Resource

Concordant but Varied Phenotypes among Duchenne Muscular Dystrophy Patient-Specific Myoblasts Derived using a Human iPSC-Based Model

In Young Choi,[1,14] HoTae Lim,[1,14] Kenneth Estrellas,[2,7] Jyothi Mula,[3,7] Tatiana V. Cohen,[3,7] Yuanfan Zhang,[2,7] Christopher J. Donnelly,[3,4,5,15] Jean-Philippe Richard,[3] Yong Jun Kim,[1,3,8] Hyesoo Kim,[1,6] Yasuhiro Kazuki,[9,10] Mitsuo Oshimura,[9] Hongmei Lisa Li,[11] Akitsu Hotta,[11,12,13] Jeffrey Rothstein,[2,3,4,5] Nicholas Maragakis,[3] Kathryn R. Wagner,[2,3,5,7,*] and Gabsang Lee[1,3,5,*]

[1]Institute for Cell Engineering
[2]Program in Cellular and Molecular Medicine
[3]Department of Neurology
[4]Brain Science Institute
[5]The Solomon H. Snyder Department of Neuroscience
[6]Stem Cell Core Facility
Johns Hopkins University School of Medicine, Baltimore, MD 21205, USA
[7]Hugo W. Moser Research Institute at Kennedy Krieger, Baltimore, MD 21205, USA
[8]Department of Pathology, College of Medicine, Kyung Hee University, 02447 Seoul, Korea
[9]Chromosome Engineering Research Center, Tottori University, Tottori, Japan
[10]Department of Biomedical Science, Institute of Regenerative Medicine and Biofunction, Graduate School of Medical Science, Tottori University, 680-0805 Tottori, Japan
[11]Center for iPS Cell Research and Application, Kyoto University, 606-8501 Kyoto, Japan
[12]iCeMS, Kyoto University, 606-8501 Kyoto, Japan
[13]PRESTO, Japan Science and Technology Agency, 332-0012 Kawaguchi, Japan
[14]Co-first author
[15]Present address: Department of Neurobiology, Live Like Lou Center for ALS Research, Brain Institute, University of Pittsburgh, School of Medicine, Pittsburgh, PA 15260, USA
*Correspondence: wagnerk@kennedykrieger.org (K.R.W.), glee48@jhmi.edu (G.L.)
http://dx.doi.org/10.1016/j.celrep.2016.05.016

SUMMARY

Duchenne muscular dystrophy (DMD) remains an intractable genetic disease. Althogh there are several animal models of DMD, there is no human cell model that carries patient-specific *DYSTROPHIN* mutations. Here, we present a human DMD model using human induced pluripotent stem cells (hiPSCs). Our model reveals concordant disease-related phenotypes with patient-dependent variation, which are partially reversed by genetic and pharmacological approaches. Our "chemical-compound-based" strategy successfully directs hiPSCs into expandable myoblasts, which exhibit a myogenic transcriptional program, forming striated contractile myofibers and participating in muscle regeneration in vivo. DMD-hiPSC-derived myoblasts show disease-related phenotypes with patient-to-patient variability, including aberrant expression of inflammation or immune-response genes and collagens, increased BMP/TGFβ signaling, and reduced fusion competence. Furthermore, by genetic correction and pharmacological "dual-SMAD" inhibition, the DMD-hiPSC-derived myoblasts and genetically corrected isogenic myoblasts form "rescued" multi-nucleated myotubes. In conclusion, our findings demonstrate the feasibility of establishing a human "DMD-in-a-dish" model using hiPSC-based disease modeling.

INTRODUCTION

Embryonic development has been successfully modeled in vitro by differentiating human pluripotent stem cells (hPSCs), including human embryonic stem cells (hESCs) and human induced pluripotent stem cells (hiPSCs). This occurs by modulating relevant signaling pathways via chemical compounds, as demonstrated in the neuroectodermal, cardiac, and endodermal lineages (Borowiak et al., 2009; Burridge et al., 2014; Chambers et al., 2009; Di Giorgio et al., 2008). Combined with a strategy to isolate homogenous populations, disease-specific hiPSC-derived cells have facilitated our understanding of the pathogenesis of human genetic disorders by providing symptom-relevant cell types in a patient-specific manner (Chen et al., 2014; Kiskinis et al., 2014; Wainger et al., 2014). This has lead researchers to validate potential therapeutic small molecules that can rescue in vitro phenotypes (Brennand et al., 2011; de Boer et al., 2014).

However, efforts such as those mentioned above have not yet been fully applied to the hiPSCs of muscular dystrophy, mainly due to the absence of a successful strategy for isolating

expandable functional myoblasts. Previous efforts to derive myogenic cells from hESCs and hiPSCs were based on the ectopic expression of myogenic transcription factors, such as *PAX3*, *PAX7*, and *MYOD1*, by viral gene delivery (Darabi et al., 2012; Tedesco et al., 2012). Although this approach can produce certain myogenic cells, the random integration of viral DNA can jeopardize disease modeling and mask any unknown potential disease phenotype. In addition, other previous methods rely on animal-derived factors and require arduous long-term culture (4 months or more) (Barberi et al., 2007). More importantly, high-purity, disease-specific myoblasts must be isolated and expanded to study their transcriptional profiles or functional deficits. Considering the high disease prevalence and severity, as well as a lack of meaningful therapies for most skeletal muscle disorders, it is critical to develop a human cellular model system.

One of the most common muscular dystrophies is Duchenne muscular dystrophy (DMD), which affects approximately 1 in 5,000 live male births. DMD is caused by mutations in *DYSTROPHIN* (Hoffman et al., 1987), and more than 1,000 different sequence variations in the culprit gene (http://www.dmd.nl) have been discovered. Patients with DMD have heterogeneous disease severity due to specific *DYSTROPHIN* mutations as well as modifier genes, as demonstrated by a wide range of loss of ambulation and end of life (Vo and McNally, 2015). Although zebrafish, mouse, and dog models have provided DMD-related data on pathogenesis, it is generally recognized that each of these models have limitations (Kornegay et al., 2012; Partridge, 2013). A DMD study using mouse embryonic stem cells (mESCs) from a DMD mouse model was published recently (Chal et al., 2015). However, it is still questionable whether any of the mESC-based studies can sufficiently model such varied severity in a mutation-dependent or patient-specific manner.

Humanized DMD models carrying patient-specific *DYSTROPHIN* mutations will be complementary to current animal models of DMD. One such potential humanized DMD cell model is DMD-specific hiPSCs. Here, we planned to establish a defined, robust, and efficient system to direct hPSCs into myogenic specification, demonstrating the feasibility of myoblast derivation from DMD-specific hiPSCs. Recapitulation of the heterogeneous severity of disease among patients could be a step toward comprehensive mechanistic studies on DMD pathogenesis. In addition, harnessing the potential of hiPSC technology may lead to a more personalized approach for DMD treatment.

RESULTS

A Defined Myogenic Specification Platform Generates a Pure and Functional Myoblast Population

To harness the potential of hPSCs, we developed a protocol to direct hPSCs into the skeletal muscle lineage. As the somite is an intermediate stage between hPSCs and myogenic progenitor cells (Bentzinger et al., 2012; Dequéant and Pourquié, 2008) (Figure S1A), we generated a *MESOGENIN1::eGFP* reporter hESC line with the CRISPR/Cas9 system (Mali et al., 2013) (Figures S1B–S1D). *MESOGENIN1* is a genetic marker for the pre-somite mesoderm fate (Fior et al., 2012). Brief treatment (4 days after day 0 of differentiation) with CHIR99021, a GSK-3β inhibitor (Bennett et al., 2002), significantly increased expression of *MESOGENIN1::eGFP* (80.8% ± 11.3% cells out of total cells in a dish), TBX6 (67.4% ± 10.4%), and PAX3 in a dose-dependent manner (Figures S1E–S1G) at day 4 and gave rise to myogenic cells expressing MyHC (MF20), MYOG, and MYOD at day 40 (30.4% ± 13.7%, 37.7% ± 5.78%, and 30.4% ± 13.70%, respectively) (Figure S1H). CHIR99021 appeared to activate the canonical WNT signaling pathway, confirmed by β-catenin translocation into the nucleus (Figure S1I). Further data analysis suggests that WNT activation and inhibition of the PI3K pathway (Figures S1J–S1L) are sufficient for induction of *MESOGENIN1::eGFP* from hPSCs. These data are partially explained by fostering myogenic specification from somite cells as well as enhanced WNT activation (Figures S1M–S1P), and they are in agreement with results of studies from other groups (Borchin et al., 2013; Chal et al., 2015; Wang et al., 2007; Xu et al., 2013). To increase the speed and efficacy of myogenic specification, we found that treatment from day 4 to day 12 with DAPT, a γ-secretase inhibitor that blocks Notch signaling (Dovey et al., 2001) (Figure 1A), promoted a robust and fast myogenic differentiation. At day 30, 63.6% ± 9.68% of cells were MF20+, and 61.5% ± 11.0% were MYOGENIN+ (Figures 1B and S1Q–S1U), which is consistent with data from recent rodent studies (Mayeuf-Louchart et al., 2014; Mourikis et al., 2012).

The resulting "CHIR99021-DAPT culture" in defined N2 media (Figure 1A) was tested on multiple hiPSC lines (>10 different clones) and consistently resulted in differentiation of myoblasts into multinucleated and spontaneously contractile myotubes (Movies S1, S2, and S3; skeletal muscle cells derived from hESC [H9] and normal hiPSCs [GM01582, GM02036]). The hESC- and hiPSC-derived myotubes in CHIR99021-DAPT culture were further characterized by transmission electron microscopy. The spontaneously contracting myotubes showed a highly organized structure, including intact sarcomeres with distinct Z-lines, M-lines, and I-bands (Figures 1C and S1V).

To determine the in vivo engraftment potential, we transplanted the dissociated CHIR99021-DAPT culture cells into the injured tibialis anterior (TA) muscle of *NOD-Rag1*^{null}*IL2rγ*^{null} (NRG) mice. 6 weeks after transplantation, immunohistochemistry performed with two human specific antibodies (human-specific Lamin A/C and human-specific Laminin) confirmed that the transplanted human myoblasts formed extensive myofibers without tumor formation (n = 33 mice) (Figure 1D, left). Importantly, a small proportion of human nuclei (human Lamin A/C +) were also observed to express PAX7 underneath a human Laminin basal lamina, indicating that some of the transplanted cells occupied the niche of adult muscle stem cells, known as satellite cells (Figure 1D, right). In contrast, no expression of human antigens was detected in sham-transplanted control mice.

To determine the presence of fusion-competent myoblasts, we re-plated the dissociated cells from the CHIR99021-DAPT culture (days 25–30). Most of the attached and surviving cells were mono-nucleated at day 2 after re-plating, and they could form multi-nucleated myotubes at day 10 after re-plating with typical striations and expression of myotube marker proteins, including DYSTROPHIN (35.55 ± 6.4% cells were positive), TITIN (37.5% ± 5.25%), and α-ACTININ (40.8% ± 9.7%, sarcomeric organization) (Figures 1E, 1F, and S1W).

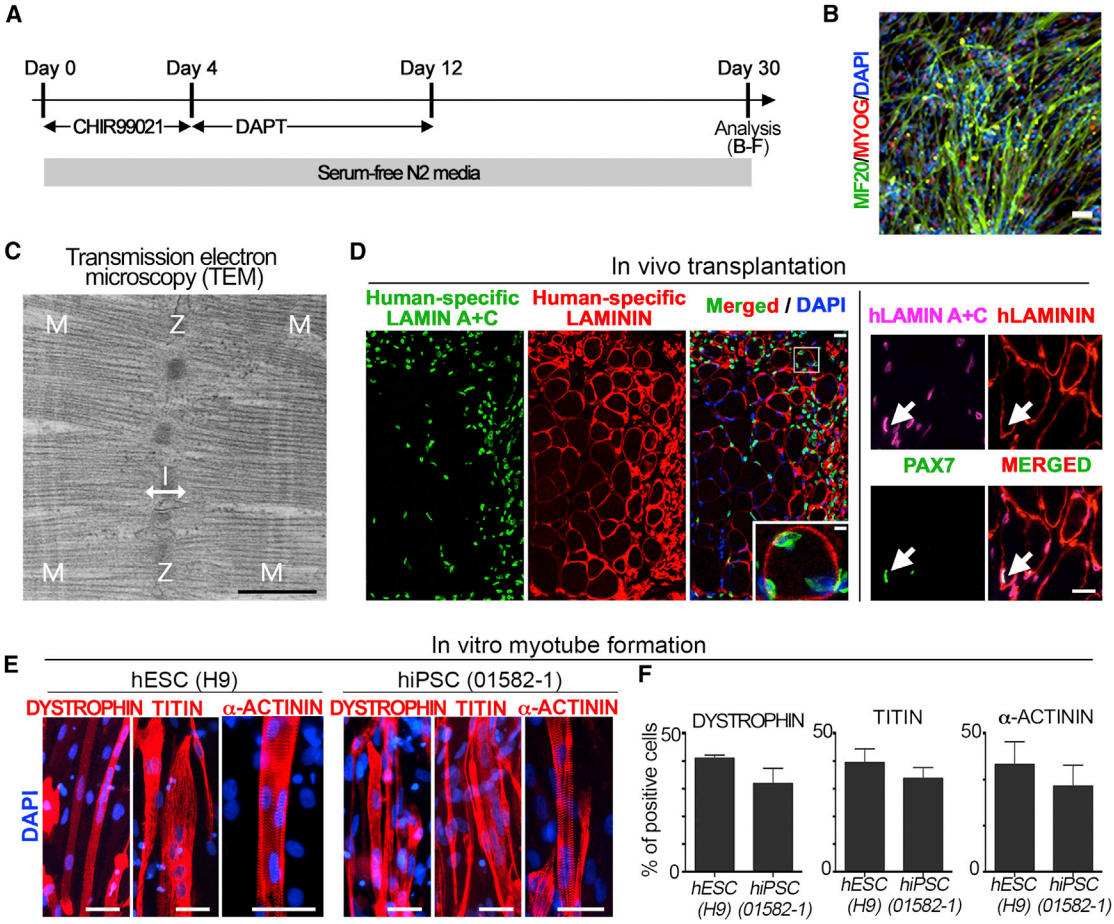

Figure 1. Characterization of Myogenic Cells Derived from hPSCs

(A) Schematic illustration of myogenic specification of hPSCs with two chemical compounds.

(B) Myogenic differentiation after CHIR99021 and DAPT treatment, determined (day 30) by expression of myosin heavy chain (MF20) and myogenic regulatory factors (MYOG).

(C) Transmission electron micrograph showing sarcomeres in contractile, mature myotubes derived from hESCs (WA09).

(D) Left: formation of numerous human, multi-nucleated myofibers by transplanted hPSC-derived skeletal muscle cells, 4 weeks after injection, confirmed with two human specific antibodies (LAMIN A+C and LAMININ). Inset shows enlarged image of a single myofiber. Right: co-expression of PAX7+ and hLAMIN A+C nucleus (white arrow) in human myofiber expressing hLAMININ.

(E) Formation of hESC- and hiPSC-derived multinucleated myotubes expressing DYSTROPHIN, TITIN, and α-ACTININ (with striation).

(F) Quantification of DYSTROPHIN, TITIN, and α-ACTININ expressing cells.

n = 3–10. Scale bars represent 50 μm, except (C) (500 ηm) and the inset of (D) (5 μm).

Isolation of fusion-competent myoblasts could pave the way for disease modeling. As shown in Figures 1E, 1F, and S1T, our CHIR99021-DAPT culture contains fusion-competent myoblasts as well as differentiated myotubes with well-organized sarcomeres. To isolate myoblasts, we tested multiple cell surface markers to facilitate fluorescence-activated cell sorting (FACS) purification of myoblasts in CHIR99021-DAPT culture. Positive selection with the NCAM (5.1H11) antibody (Webster et al., 1988) combined with negative selection using the HNK1 antibody (Figures 2A and S2A) enriched skeletal muscle progenitor cells. This determination was based upon significantly increased expression levels of *MYOD1*, *MYOG*, and MyHC (Figures 2B, 2C, S2B, and S2C) in the NCAM+/HNK1− fraction over the NCAM− or NCAM+/HNK1+ fractions. Furthermore, single-cell qRT-PCR showed that 98% (95 out of 96) of single NCAM+/HNK1− cells had higher expression of *MYOG* and *PAX7* than a sample of human fetal skeletal muscle and undifferentiated hESCs (Figures S2D and S2E).

To identify the global mRNA profiles, we performed unbiased gene expression analysis, which showed a hierarchical clustering between the hPSC-derived NCAM+/HNK1− population and fetal skeletal muscle (18 to 19 weeks of gestation) over undifferentiated hESCs (Figure 2D). Transcripts highly enriched in the NCAM+/HNK1− fraction included key markers of skeletal muscle structure development (Millay et al., 2013; Wang et al., 1979; Wohlgemuth et al., 2007) and key transcription factors (L'Honoré et al., 2007; Martin et al., 1993) (Figure 2E). Gene

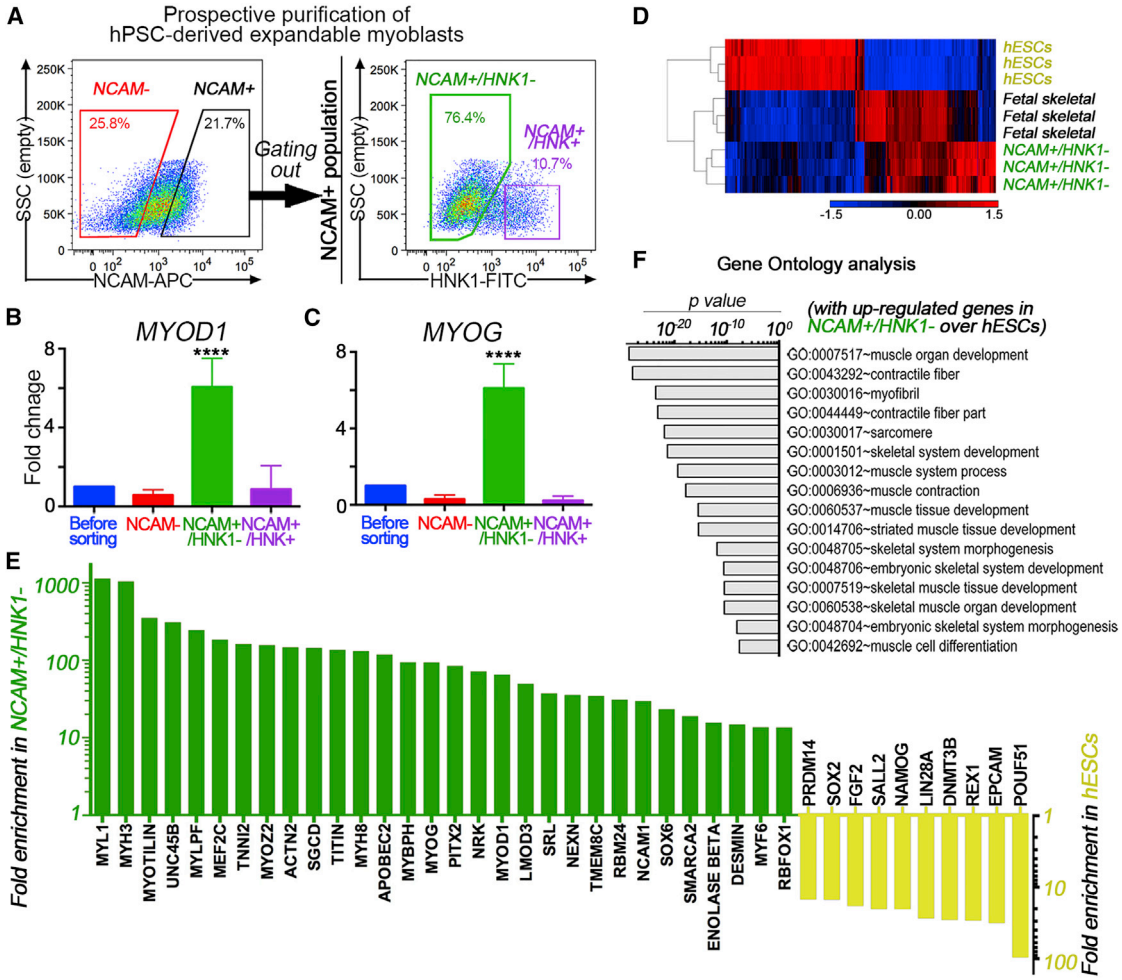

Figure 2. FACS Purification of Functional Myoblasts Cells

(A) Representative FACS plots for NCAM+/HNK1− cell population.

(B and C) qRT-PCR confirming expression of MYOD1 (B) and MYOG (C) in post-sorted cells.

(D) Clustered heatmap of global gene expression values comparing NCAM+/HNK1−, human fetal skeletal muscle (18 to 19 weeks), and undifferentiated hESCs (hESC), using Partek program (Pearson correlation). The plot is rank-ordered with pluripotent-specific genes on the left and skeletal muscle specific genes on the right.

(E) Graph of the changes in gene expression levels as assessed by microarray analysis: increased in NCAM+/HNK1− (green) and decreased in undifferentiated hESCs populations (yellow) compared to each other.

(F) Gene ontology (DAVID) analysis of upregulated transcripts in NCAM+/HNK1− population.

****$p \leq 0.0001$. One-way ANOVA followed by Newman-Keuls test. n = 3–5. All values represent mean and SD.

ontology (GO) analysis revealed statistically significant over-representation of GO terms among the upregulated genes in the NCAM+/HNK1− fraction, including those of "embryonic skeletal muscle development" ($p = 4.52 \times 10^{-22}$), "muscle structure system" ($p = 2.10 \times 10^{-29}$), and "muscle contraction" ($p = 2.61 \times 10^{-24}$) (Figure 2F). The gene expression array results were confirmed by qRT-PCR with primer sets for selected genes (Figure S2F). The isolated NCAM+/HNK1− population was markedly proliferative during exposure to expansion-permissive conditions for 6 weeks and could be easily expanded up to hundreds of millions of cells (a population doubling time for hESC and hiPSCs of 50.8 ± 18.5 hr and 47.9 ± 17.0 hr, respectively) (Figure S2G). The hiPSC-derived myoblasts could be successfully cryopreserved and maintained their myotube-forming potential upon thawing (Figure S2H).

Generation of Myoblasts from hiPSCs of Duchenne Muscular Dystrophy

To test whether our myoblast specification and isolation protocol could be applied to hiPSCs derived from DMD patients, we generated patient-specific hiPSCs from five different genotypes (Table 1 and Figures S3A–S3E). In order to find transcriptional changes between NCAM+/HNK1− cells (Figure S3F) of DMD-hiPSC (GM05169, exon 4–43 deletion) and the control (healthy)-hiPSC population, we applied unbiased global transcription analysis and subsequent GO analysis (Figure 3A). The

Table 1. Details of Fibroblasts Used for Generation of DMD-hiPSC Lines

ID in Coriell Catalog	Description	Mutations	Age (yr)
GM05169	DMD (deletion)	EX4-43DEL	9
GM05127	DMD (non-sense mutation)	c.5533G > T, p.E1845X	18
GM04327	DMD (duplication)	EX5-7DUP	23
GM03781	DMD (deletion)	EX3-17DEL	11
GM03783	DMD (deletion)	EX3-17DEL	10

differentially upregulated genes in NCAM+/HNK1− cells of the DMD-hiPSC population (hereafter referred to as DMD-myoblasts) were largely classified into wound healing, inflammation, and signaling pathways. To validate these findings in different genotypes and mutations in DMD patient hiPSCs (Table 1), we chose a set of significantly upregulated genes in DMD-myoblasts (fold change $\geq$ 2-fold; corrected p value of 0.05), which included 17 over-represented genes in the five categories mentioned above, to perform qRT-PCR analysis. Using additional DMD-hiPSC lines with different mutations (two exon 3–17 deletion, one exon 5–7 duplication, and one nonsense mutation; at least three iPSC clones per genotypes), we generated myoblasts from each clone of DMD-hiPSC lines using previously mentioned protocols (Figure S1) of myogenic specification and FACS purification. No DYSTROPHIN protein was detectable in the DMD-hiPSC-derived myoblasts using western blot and immunohistochemistry (Figures S3G and S3H), whereas control hPSC-derived myoblasts showed detectable levels of DYSTROPHIN expression (Figure S3I). Furthermore, DMD-hiPSC-derived myoblasts showed distinctively different myogenic marker gene expression patterns than fibroblasts (Figure S3J). In vivo transplantation experiments with two different mouse strains, NOD-Rag1^{null}IL2rγ^{null} mice (immuno-deficient healthy recipients) and NOD-SCID-IL2rγ^{null}-mdx^{4Cv} mice (immuno-deficient mdx mice lacking dystrophin) (Arpke et al., 2013), demonstrated that myogenic culture of DMD-hiPSCs could participate in muscle regeneration processes after cardiotoxin injury (Figure S3K).

The different DMD-myoblasts each had varying levels of gene expression in the DMD qRT-PCR analysis, although all assayed genes were aberrantly expressed in DMD-myoblasts compared to control hiPSCs. In particular, all lines showed upregulated expression of BMP4 and TGFβ genes (Figure 3B). Increased levels of BMP4 and TGFβ signaling were confirmed by a significantly increased nuclear localization of phosphorylated SMAD (pSMAD 1/5 and 2/3) in DMD-myoblasts compared to control myoblasts (Figures 3C, 3D, and S3L). We also found increased protein expression levels of interleukin 6 and 8 and collagen 3 in DMD-myoblasts, whereas the expression level of collagen 1 remained unchanged (Figures 3E–3G and S3M). Interestingly, myoblasts from individual DMD-hiPSC lines showed different patterns. For example, they all had higher levels of nuclear localized phospho-SMAD 1/5 and 2/3, but expression levels of interleukin 6 and 8 and collagen 3 were varied among different DMD-hiPSC lines. Furthermore, analysis of myotube formation as measured by the fusion index (the ratio of number of nuclei inside DESMIN+ myotubes to the number of total nuclei × 100) showed that all the DMD-myoblasts from different DMD-hiPSC lines had decreased myotube formation compared to control myoblasts ($p < 0.0001$) (Figures 3H and 3I). To test whether this observation was specific to the DMD-myoblasts, we compared the hiPSC lines we developed from facioscapulohumeral muscular dystrophy (FSHD) and amyotrophic lateral sclerosis (ALS, *C9ORF72* mutation) (Figures S3A–S3D). Myoblast cultures derived from hiPSC lines of FSHD and ALS could form myotubes with expression of disease biomarkers (Figures S3N–S3P). As shown in Movie S4, we often found spontaneously twitching cells during myogenic specification of ALS-hiPSCs, but we have not found any spontaneously contracting cells during DMD-hiPSC differentiation (n = 71 repeats). To confirm our findings, we used a previously published protocol (Shelton et al., 2014) and showed robust myogenic specification (comparable levels to our protocol) in healthy control hPSCs (Figures S3Q and S3R). However, there were differential transcriptional profiles of DMD-hiPSCs (Figure S3S). In addition, the DMD-hiPSC-derived myoblasts showed aberrant myotube formation with many branched arms, reminiscent of another group's study using mdx mESCs (Chal et al., 2015) (Figure S3T).

Our data suggest that myoblasts of DMD-hiPSCs display transcriptional, translational, and functional in vitro phenotypes. After confirming the transcriptional and translational phenotypes of DMD-myoblasts, we hypothesized that there might be a significant correlation among the list of aberrantly expressed genes (Figure 3B). A correlation heatmap was generated using the gene-to-gene Pearson correlations for the 16 genes initially chosen from global transcriptional analysis (Figure 3J). Among the positively co-correlated genes, SPP1, BMP4, CASPASE1, BMP2, and TGFβ3 formed the clearest cluster. Furthermore, additional correlation analysis (Table 2) confirmed a statistically significant correlation (p value, 0.0211 $\sim$ <0.0001) between SPP1 and the other 12 genes. Interestingly, SPP1 (Osteopontin) has been shown to be a potent genetic modifier of disease severity in DMD (Pegoraro et al., 2011; Zatz et al., 2014).

Rescuing Phenotypes of DMD-Myoblasts by Genetic Restoration of *DYSTROPHIN*

To restore the genetic deficiency of the exon 4–43 deletion of one of the DMD mutations, we employed the human artificial chromosome (HAC) technique (Kazuki et al., 2010). The HAC technique was used because conventional gene targeting approaches were not feasible due to the size of the DNA to be delivered. We reprogrammed genetically corrected DMD fibroblasts (GM05169 carry HAC with 2.4 Mb entire genomic *DYSTROPHIN*, renamed DF160) into hiPSCs (Figures S4A and S4B). After confirmation of normal karyotype and presence of the HAC (Figures S4C and S4D), the myogenic culture of corrected DMD-hiPSCs was transplanted into NRG and NSG-mdx^{4Cv} mice. We found comparable levels of human myofiber formation in both in vivo environments (Figures S4E–S4G). These data are supported by recent reports from other groups (Boldrin et al., 2015; Dumont et al., 2015). FACS-purified myoblasts from the corrected DMD-hiPSCs (referred to as "corrected DMD-myoblasts") showed (Figure 4A) reversed gene expression profiles in our DMD qRT-PCR assay (Figure 4B). Using an

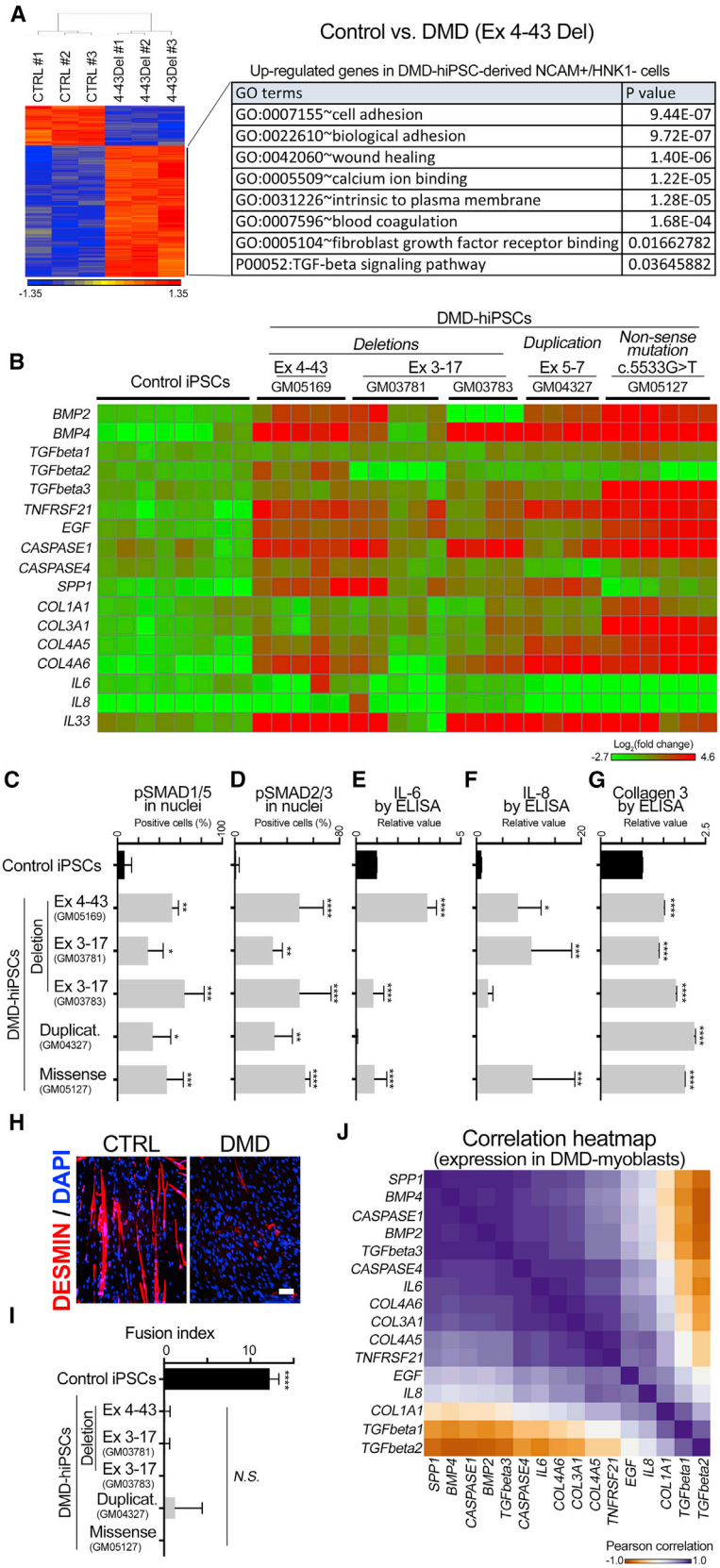

Figure 3. DMD-hiPSC-Derived Myoblasts Show Disease-Related Phenotypes

(A) Unsupervised clustered heatmap of global gene expression values comparing control (CTRL) and DMD-hiPSC-derived myoblasts (DMD-myoblasts) (after NCAM+/HNK1− purification) and gene ontology (DAVID and IPA/Ingenuity) analysis of transcripts that were upregulated in DMD as opposed to downregulated in control (left lower panel) transcripts in control myoblasts.

(B) Heatmap of DMD qRT-PCR analysis with selected represented genes. The value is acquired after normalization by GAPDH value and fold change by the mean value of control hiPSCs. Each box represents different clones of the genotypes and biological repeats of the myoblast isolation.

(C–G) Nuclear localization of phosphorylated SMAD (pSMAD) proteins and expression levels of interleukin 6 and 8, and collagen 3 found in myoblasts (after NCAM+/HNK1− purification) of multiple DMD-hiPSC lines.

(H and I) Impaired myotube formation in DMD-myoblasts. (H) Representative images showing DESMIN staining. (I) Decreased level of fusion index (calculated as ratio of number of nuclei inside myotubes to the number of total nuclei × 100 after myotube formation).

(J) Pearson correlation heatmap among the genes listed in (B) shows the Pearson correlation coefficients of expression levels of each selected gene among DMD-myoblasts of five different patient hiPSC lines. Color key from brown to purple indicates correlation from low to high, respectively. The normalized expression values of those genes in were used for calculation of correlation matrix.

*$p \leq 0.05$, **$p \leq 0.01$, ***$p \leq 0.001$, ****$p \leq 0.0001$. One-way ANOVA followed by Newman-Keuls test. *N.S.*, not significantly different. n = 3–11. All values represent mean and SD. Scale bar in (H) represents 50 μm.

Table 2. Correlation between SPP Expression and Other "Potentially Culprit Genes"

	r	95% Confidence Interval	R squared	p (Two-Tailed)	p Value Summary	Significant? (Alpha = 0.05)
SPP1 versus BMP2	0.974	0.9071 to 0.9929	0.9486	<0.0001	****	Yes
SPP1 versus BMP4	0.9851	0.9461 to 0.9959	0.9704	<0.0001	****	Yes
SPP1 versus TGFB1	−0.6537	−0.8927 to −0.1278	0.4274	0.0211	*	Yes
SPP1 versus TGFB2	−0.8336	−0.9520 to −0.4978	0.6948	0.0008	***	Yes
SPP1 versus TGFB3	0.9703	0.8945 to 0.9919	0.9415	<0.0001	****	Yes
SPP1 versus TNFRSF21	0.7023	0.2151 to 0.9096	0.4932	0.0109	*	Yes
SPP1 versus EGF	0.4151	−0.2085 to 0.7987	0.1723	0.1797	ns	No
SPP1 versus CASPASE1	0.9839	0.9416 to 0.9956	0.968	<0.0001	****	Yes
SPP1 versus CASPASE4	0.9397	0.7942 to 0.9833	0.8831	<0.0001	****	Yes
SPP1 versus COL1A1	−0.2073	−0.6981 to 0.4161	0.04297	0.518	ns	No
SPP1 versus COL3A1	0.849	0.5365 to 0.9567	0.7208	0.0005	***	Yes
SPP1 versus COL4A5	0.7275	0.2637 to 0.9181	0.5293	0.0073	**	Yes
SPP1 versus COL4A6	0.8846	0.6312 to 0.9674	0.7826	0.0001	***	Yes
SPP1 versus IL6	0.8993	0.6725 to 0.9717	0.8088	<0.0001	****	Yes
SPP1 versus IL8	0.2953	−0.3354 to 0.7433	0.08722	0.3514	ns	No

unsupervised hierarchically clustering approach, gene expression profiles of corrected DMD-myoblasts were closer to that of control (healthy) myoblasts but further from uncorrected DMD-myoblasts. The increased levels of nuclear localization of phosphorylated SMAD (pSMAD) and expression of interleukin 6 and 8 and collagen 3 were reversed in the corrected DMD-myoblasts (NCAM+/HNK1− cells) (Figures 4C–4G), whereas the expression level of collagen 1 remained unchanged (Figure S4H). Additionally, using μ-*DYSTROPHIN* (Scott et al., 2002) and three different gene correction approaches (−18 bp ExonSkip, knockin by TALEN, and knockin by CRISPR) (Li et al., 2015), we found that the transcriptional and functional aberrations were partially rescued in DMD-myoblasts (NCAM+/HNK1− cells) (Figures S4I–S4L). More importantly, the fusion index of the corrected DMD-myoblasts was significantly higher ($p < 0.0001$) than that of DMD-myoblasts, but it was significantly lower than that of control myoblasts ($p < 0.05$) (Figure 4H). Unlike uncorrected DMD-hiPSCs, which had a limited level of DESMIN expression (Figure 3H), the multinucleated myotubes of corrected DMD-hiPSCs expressed DYSTROPHIN, DESMIN, and MYOSIN LIGHT CHAIN-1 (Figure 4I).

Pharmacological Inhibition of SMAD Signaling Facilitates Formation of "Rescued" Myotubes

To find pharmacological rescue of the in vitro phenotypes, we focused on aberrant BMP and TGFβ signaling indicated by increased nuclear localization of pSMAD proteins in DMD-myoblasts (Figures 3C and 3D). We detected increased levels of BMP4 in the conditioned media (CM) of DMD-myoblasts (Figure S5A). Furthermore, we tested the effects of CM from DMD-myoblasts on control myoblasts and found significantly decreased myotube formation and significantly decreased expression levels of *MYOG* and *MYOD1* (Figures S5B and S5C) compared to those of the CM from control-myoblasts. The effects of CM from DMD-myoblasts were reproduced by treatment with BMP4 protein in the culture media, which were reversed by treatment with "dual-SMAD" inhibition compounds (Figure S5D) (LDN+SB: LDN193189 and SB431542). These data suggest that pharmacological rescue can mitigate the effects of inhibitory cytokines in DMD-myoblasts. We tested this hypothesis in DMD-myoblasts and found that treatment with the dual-SMAD inhibition compounds (LDN+SB) reversed the levels of increased nuclear localization of pSMAD protein and expression of interleukin 6 and 8 and collagen 3 (Figures 5A–5E). In addition, the LDN+SB treatment rescued the fusion defects in DMD-myoblasts with four out of five mutations (Figure 5F), but it did not reverse the fusion defects in DMD-myoblasts with the exon 5–7 duplication (GM04327). These data indicated that pharmacological inhibition of SMAD signaling could rescue DMD-related phenotypes in DMD-myoblasts of some patients and restore the functional deficit, albeit with less efficiency.

Next, we determined whether the genetically corrected DMD-myoblasts could fuse with DMD-myoblasts in vitro, thus mimicking the microenvironment of a DMD patient receiving a transplant of genetically correct autologous myoblasts. Genetically corrected DMD-myoblasts (DF160) were transfected with eGFP (marking the cytoplasm as green), and uncorrected DMD-myoblasts (GM05169) were transfected with nuclear RFP (marking the nuclei as red). The two cell lines were then co-cultured to permit myotube fusion (Figure 5G). Some of the GFP+ myotubes contained RFP+ nuclei, demonstrating the formation of rescued myotubes arising from fusion of corrected DMD-myoblasts and non-corrected DMD-myoblasts. The number of nuclei participating in the formation of rescued myotubes was calculated with a "rescued fusion index" (calculated as the ratio of number of nuclei inside GFP+/RFP+ rescued myotubes to the number of total nuclei × 100 after myotube formation). Importantly, the rescued fusion index between corrected DMD-myoblasts and non-corrected DMD-myoblasts was significantly increased upon treatment with dual-SMAD inhibition compounds (Figure 5H).

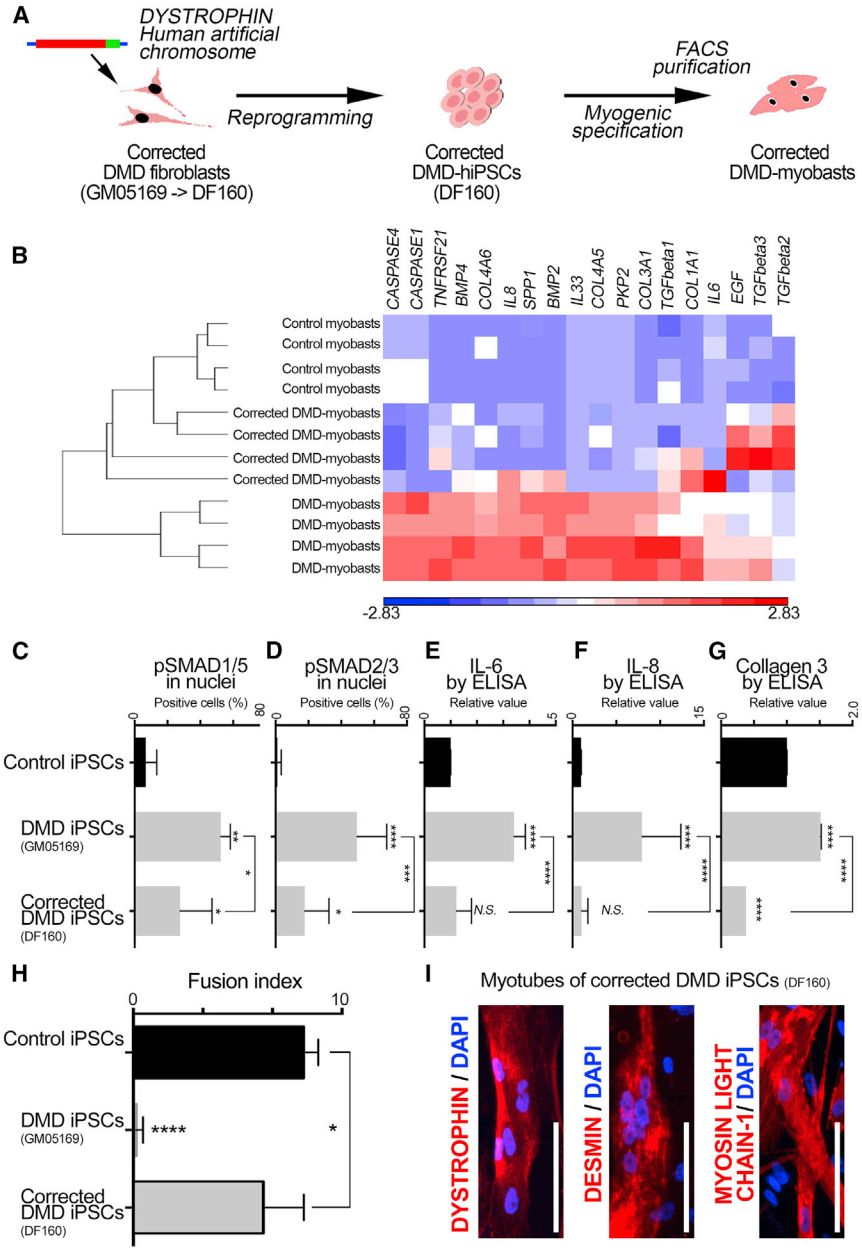

Figure 4. Genetic Rescue of DMD-Related Features

(A) Introducing human artificial chromosome (HAC) carrying full-length human DYSTROPHIN gene (DYSTROPHIN-HAC) into fibroblasts (before GM05169, after introducing, DF160), followed by reprogramming into hiPSCs, and subsequent myogenic specification into corrected DMD-myoblasts.

(B) Unsupervised clustered heatmap of DMD qRT-PCR assay with corrected myoblasts (after NCAM+/HNK1− purification) showed reversed transcription profile, using Partek program (Euclidean distances as the distance measure).

(C–G) Nuclear localization of phosphorylated SMAD (pSMAD) proteins and expression levels of interleukin 6 and 8, and collagen 3 found in myoblasts (after NCAM+/HNK1− purification) of rescued hiPSC line (DF160). Impaired myotube formation in DMD-myoblasts, determined at day 10 after myotube induction.

(H and I) Increased fusion rate (H) and formation of myotubes from DF160 hiPSCs, expressing DYSTROPHIN, DESMIN, and MYOSIN LIGHT CHAIN-1 (I).

*p ≤ 0.05, **p ≤ 0.01, ***p ≤ 0.001, ****p ≤ 0.0001. One-way ANOVA followed by Newman-Keuls test. n = 3–6. All values represent mean and SD.

DISCUSSION

We have demonstrated that a myogenic specification protocol employing two small molecules (CHIR99021 and DAPT) is sufficient to direct multiple hPSC lines (13 different genotypes, including 3 different disease-specific hiPSC lines) into myogenic lineages in approximately 30 days. The hPSC-derived myoblasts can be isolated by FACS, and their functional and molecular characterization confirmed their myogenic properties, such as authentic myogenic transcriptional program, formation of striated contractile myofibers, highly organized ultra-structure, and in vivo engraftment capability. Furthermore, this system was readily applied to DMD-specific hiPSCs with multiple genetic variations (three different deletion types, one duplication, and one nonsense mutation), successfully generating DMD-myoblasts presenting DMD-related phenotypes including altered transcriptional profiles, aberrant intracellular signaling, and defective myotube formation. These DMD phenotypes were partially reversed by genetic and pharmacological approaches, resulting in the formation of rescued myotubes between DMD-myoblasts and their genetically corrected isogenic ones. Our myoblast purification and defined culture methods have enabled us to set up a humanized DMD model system to study multiple aspects of DMD pathogenesis.

The induction of myogenic specification of hESCs and hiPSCs by CHIR99021 treatment has previously been reported by other investigators (Shelton et al., 2014). However, the underlying mechanisms of CHIR99021 activity remain unresolved. In our studies using the MESOGENIN1::eGFP reporter hESC line, which was generated by CRISPR/Cas9-mediated gene-targeting, we found that activation of the WNT pathway and inhibition of the PI3K pathway are needed for directing hESCs and hiPSCs into the somite stage (MESOGENIN1::eGFP+ population), suggesting possible off-target effects of CHIR99021. Our data also indicate that inhibition of the Notch signaling pathway is critical to increase and accelerate the myogenic program of hESC/hiPSC-derived somite cells, consistent with a recent study

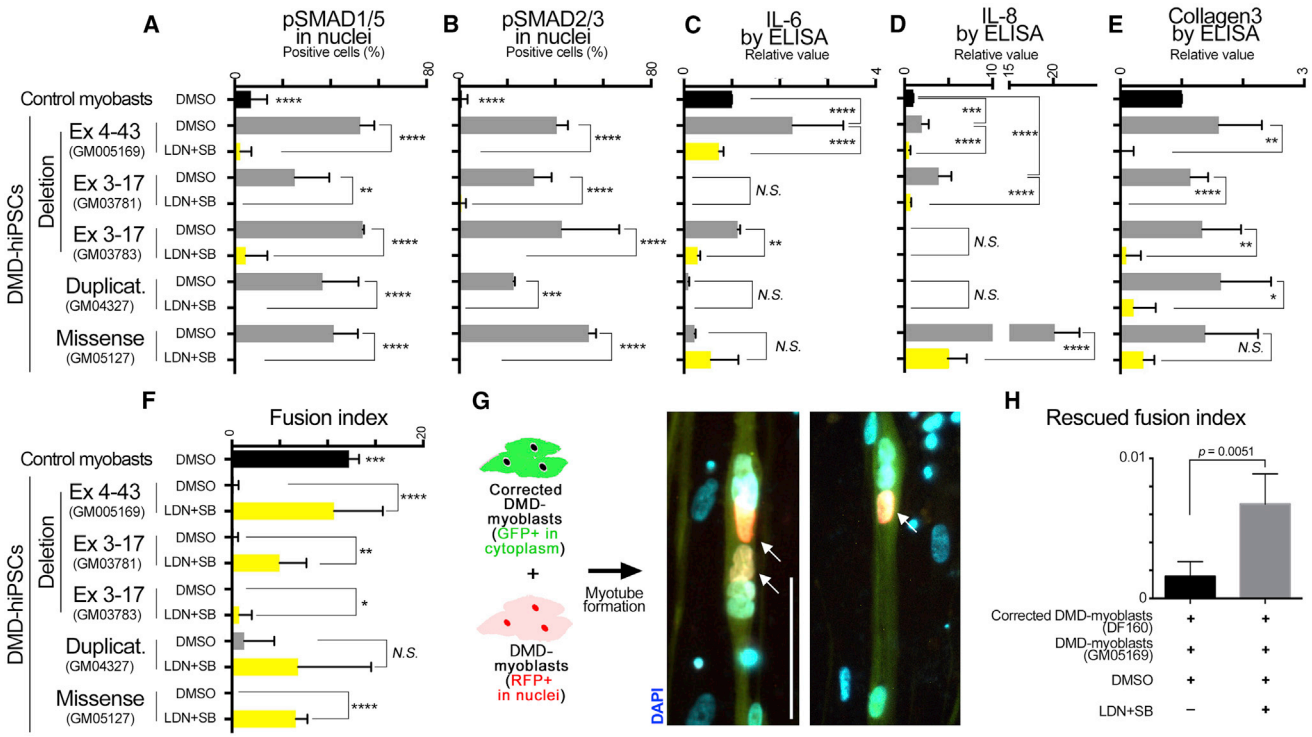

Figure 5. Pharmacological Inhibition of SMAD Signaling Facilitates Formation of "Rescued" Myotubes

(A–F) The "dual-SMAD inhibition" compounds (LDN193189 + SB431542 = LDN+SB) treatment partially reverses the localization of phosphorylated SMAD (pSMAD) proteins (A and B), expression levels of interleukin 6 (C) and 8 (D), collagen 3 (E), and myotube formation (F) in myoblasts (after NCAM+/HNK1− purification) of multiple DMD-hiPSC lines.

(G and H) GFP-labeled corrected DMD-myoblasts were co-cultured with RFP-labeled (nuclei localized) DMD-myoblasts for formation of rescued myotubes as shown in two independent images with a single GFP-labeled myotube containing RFP-labeled nuclei (G). (H) Ratio of rescued myotube formation was significantly enhanced upon treatment with LDN+SB. The "rescued fusion index" was calculated as the ratio of number of nuclei inside GFP+/RFP+ rescued myotubes to the number of total nuclei × 100 after myotube formation.

*p ≤ 0.05, **p ≤ 0.01, ***p ≤ 0.001, ****p ≤ 0.0001. One-way ANOVA followed by Newman-Keuls test, except (F), t test between DMSO and LDN+SB treatment per genotype. n = 3–6. All values represent mean and SD. All scale bars represent 50 μm.

(Mayeuf-Louchart et al., 2014) showing the significance of Notch signaling on the fate decision processes of somite cells.

The myotubes generated using our culturing method were often found to spontaneously contract in vitro and possessed a highly systematized ultrastructure resembling that of in vivo skeletal muscle. Indeed, in vivo experiments with the myogenic cells of hESCs and hiPSCs demonstrated that they efficiently participated in the process of murine muscle regeneration. Importantly, a few transplanted human cells expressing PAX7 could be found in the satellite cell niche beneath the basal lamina.

Another important finding in our current study is the establishment of an isolation strategy of expandable myoblasts from a heterogeneous hiPSCs culture. After approximately 30 days of myogenic specification, we observed that the culture dishes contained different types of cells, including spontaneously twitching myofibers and myotubes, myoblasts, neurons, and fibroblasts. Among this diversity of cells, only some of them were mono-nucleated myoblasts, which can be FACS-purified by using NCAM and HNK1 antibodies. This FACS-purification strategy was readily applied to multiple hiPSC lines, and the yields were comparable among different genotypes of hESCs and hiPSCs, including DMD-hiPSCs. Furthermore, the FACS-purified myoblasts can be expanded up to the hundreds of millions of cells, and they are easily cryo-preserved without losing fusion competence. Combined with the xeno-free culture condition (defined media condition and compound based specification), our protocol could be extended to large-scale compound screening efforts and eventually to myoblast transplantation to patients. Additional studies are necessary to reveal the detailed molecular mechanisms governing the fate of each cellular stage during human myogenesis, to comprehensively quantify PAX7+ human transplanted cells, and to monitor the long-term in vivo behaviors of transplanted cells.

The DMD phenotypes in our present study, including increased levels of BMP4 and TGFβ signaling, aberrant expression of interleukins and the collagen genes, and fusion defects, are supported by previous studies of DMD animal models and myoblast cultures derived from DMD patient biopsy samples (Cesana et al., 2011; Hartel et al., 2001; Jasmin et al., 1984; Ng et al., 2012; Porter et al., 2002). Our present study implies that secreted proteins might be responsible for the defective

in vitro fusion of DMD-myoblasts. This finding was confirmed in other experiments, such as treatment of control-myoblast cultures with CM of DMD-myoblasts and co-cultures between control-myoblasts and DMD-myoblasts, and it was partially reversed by dual-SMAD inhibition. Importantly, upon dual-SMAD inhibition, genetically corrected DMD-myoblasts can form significantly increased numbers of rescued myotubes containing nuclei of DMD-myoblasts. This rescued myotube culture can be useful to study myoblast transplantation efficiency. More than a decade ago, encouraged by successful transplantation studies with *mdx* rodent models (Karpati et al., 1993; Partridge et al., 1989), researchers attempted clinical trials of allogenic myoblast transplantation for the treatment of DMD, but unfortunately the results were disappointing (Karpati et al., 1993; Mendell et al., 1995; Skuk et al., 2007). Although more recent attempts at human myoblast transplantation have achieved some DYSTROPHIN expression, subsequent biopsies have shown severe substitution by fibrosis and adipose tissue (Gussoni et al., 1992). There is little understanding as to why transplanted healthy myoblasts perform so poorly. Although rapid cell death of transplanted healthy myoblasts (Fan et al., 1996) and immune rejection have been suggested as reasons for low transplant efficiency, an ''unfavorable'' or ''hostile'' microenvironment of the DMD host likely plays a significant role (Gussoni et al., 1997). Although the low level of rescued myotube formation must be improved in future studies, our humanized DMD myoblast model will be useful to reconstruct a microenvironment of DMD lesions receiving autologous and genetically corrected myoblasts.

DMD-myoblasts from four patients were rescued upon pharmacological dual-SMAD inhibition, but DMD-myoblasts with exon 5–7 duplication (GM04327) were not able to be rescued. These data suggest that patient-specific disparities in DMD manifestation might be modeled in cell culture. It remains to be determined why DMD-myoblasts originating from different patients display varied phenotypes and responses to pharmacological rescue; however, these data might be relevant to the varied severity and progression of the disease symptoms among patients and potentially the response to different therapeutic reagents (Pegoraro et al., 2011; Zatz et al., 2014). For example, our data show that SPP1/Osteopontin expression levels in DMD-myoblasts of different patients are significantly correlated with most of the elevated expression levels of the ''pathogenic candidate genes.'' The relationship and potential mechanism between the expression level of SPP1/Osteopontin and the clinical severity and progression will be investigated in future studies with DMD-myoblasts of large numbers of patient groups. In particular, the genetic labeling (e.g., PAX7::GFP reporter DMD-hiPSC lines) system will be very important for reliable isolation of putative skeletal muscle stem cells from DMD-hiPSC lines.

Another interesting question is how DMD-myoblasts show relevant phenotypes even before initiation of DYSTROPHIN protein expression. We have found that *DYSTROPHIN* transcription occurs in myoblasts (Figure 3I) before myotube formation, but the protein is not detected in the myoblast stage. Future studies will be focused to uncover a possible unknown function of DYSTROPHIN transcript or protein with more precise and sensitive detection methodologies. Moreover, our in vivo experiments demonstrate that myogenic cells of DMD-hiPSCs can form human myofibers in healthy and mdx mouse models. Our in vitro human model of DMD-myoblasts can be used to model the cellular conditions of DMD patient pathology and will be useful for understanding patient-specific disparities.

In conclusion, our data demonstrate the feasibility of generating and isolating expandable myoblasts from disease-hiPSCs in a fast, efficient, and defined manner. We have gained insight into the disease mechanism underlying DMD and present a model for studying the processes for using iPSCs as therapies for DMD.

EXPERIMENTAL PROCEDURES

Cell Culture

hESCs (H9, WiCell) and hiPSCs were cultured using standard protocols. The hESC lines and hiPSC lines were cultured with mouse embryonic fibroblasts (MEFs) (GlobalStem, or AppliedStemCell) pre-plated at 12,000–15,000 cells/cm^2. Medium contained DMEM/F12, 20% knockout serum replacement, 1 mM L-glutamine, 100 μM MEM non-essential amino acids, and 0.1 mM β-mercaptoethanol. 10 ng/mL of FGF-2 was added after sterile filtration, and cells were fed daily, and passaged weekly, using 6 U/mL dispase or mechanically.

Generation of hiPSCs

The ALS patient fibroblasts (JH078 [C9ORF72] and GO013 [SOD1 A4V]) were collected at Johns Hopkins Hospital with patient consent (IRB protocol: ''Skin biopsies to generate cell lines for study of Amyotrophic Lateral Sclerosis,'' NA_00021979). Primary FSHD myoblasts (05Bdel) were obtained from the Senator Paul D. Wellstone Muscular Dystrophy Cooperative Research Center for FSHD Research. Other fibroblasts (Table 1) were purchased from Coriell with appropriate Material Transfer Agreement documents. Genetically corrected DMD fibroblasts (DF160) were previously generated by transferring the HAC with the entire DYSTROPHIN gene into DMD fibroblasts (GM05169). Human cells were cultured in DMEM media containing 10% fetal bovine serum (FBS). Fibroblasts were plated onto 24-well plates and then reprogrammed with CytoTune-iPS Sendai Reprogramming Kit (Invitrogen) using our standard protocol. After 9 days, cells were put on MEF feeder medium with Y-27632 and then grown.

Myogenic Differentiation of hESCs and hiPSCs

MEF-conditioned N2 media is used for initial stage of myogenic specification. Briefly, MEFs were plated at a density of 50,000 cells/cm^2 in a T-225 flask. The next day, the cells are washed once with PBS before adding 100 ml of N2 medium. MEF-conditioned N2 media were harvested after 24 hr of incubation. For myogenic specification, hESCs and hiPSCs were rendered to single cells using incubation of Accutase for 20 min, and plated on a gelatin-coated dish for 10 min to remove MEFs. Non-adherent cells (mostly hESCs and hiPSCs) were collected, counted, and plated on a 1% Geltrex-coated dish (1 hr coating), at a density of 1.5 × 10^5 cells per well of a 24-well plate, in the presence of filtered MEF-conditioned N2 media containing 10 ng/ml of FGF-2 and 10 μM of Y-27632 (Cayman Chemical) (day 0). From the next day (day 1) (60% ~ 70% of confluence), N2 media with CHIR99021 (3 μM) was added and media were changed at every other day. At day 4, N2 media with DAPT (10 μM) treatment were added until day 12. BIO (30–250 nM), lithium chloride (20 μM to 20 mM), Kenpallone (1–10 μM), SB 216763 (1–10 μM), WNT-1 (10–100 ng/ml), WNT-3A (10–100 ng/ml), WNT-7A (10–100 ng/ml), SBE13 hydrochloride (0.1 nM to 10 μM), and OTSSP167 hydrochloride (0.1–10 nM) were tested during day 1 to day 4, as well as during day 4 to day 8. The N2 medium contains DMEM/F12 powder, glucose, sodium bicarbonate, insulin, putrescine, progesterone, sodium selenite, and transferrin.

Statistical Analysis

All statistical analyses were performed using Graph Pad Prism software (version 6.0). Values are from at least three independent experiments, with

multiple replicates each, and reported as mean ± SEM. Comparisons among groups were performed either by one-way ANOVA followed by Newman-Keuls test or by a t test. Statistical significance was assigned for $p < 0.05$.

ACCESSION NUMBERS

The accession number for the microarray data reported in this paper is GEO: GSE70955.

SUPPLEMENTAL INFORMATION

Supplemental Information includes five figures, two tables, and four movies and can be found with this article online at http://dx.doi.org/10.1016/j.celrep.2016.05.016.

AUTHOR CONTRIBUTIONS

Conceptualization, G.L., I.Y.C., and H.L.; Methodology, G.L., K.R.W., I.Y.C., and H.L.; Investigation, I.Y.C., H.L., K.E., Y.Z., J.M., T.V.C., and C.J.D.; Resources, J.-P.R., Y.J.K., H.K., Y.J.K., M.O., H.L.L., A.H., J.R., and N.M.; Writing – Original Draft, G.L., I.Y.C., and H.L.; Writing – Review & Editing, G.L., I.Y.C., H.L., K.E., J.M., T.V.C., Y.Z., C.J.D, J.-P.R., Y.J.K., H.K., Y.JK., M.O., H.L.L., A.H., J.R., N.M., and K.R.W.; Supervision, G.L. and K.R.W.; Funding Acquisition, G.L. and K.R.W.

ACKNOWLEDGMENTS

We would like to thank the members of the G.L. lab for valuable discussions of the manuscript. We thank the Developmental Studies Hybridoma Bank for antibodies and the Senator Paul D. Wellstone Muscular Dystrophy Cooperative Research Center for FSHD Research for providing FSHD primary cells. We are grateful to Mr. Conover Talbot Jr. for the microarray analysis, Ms. Barbara Smith for the TEM studies, and Dr. Michael Kyba for sharing NSG-mdx^{4Cv}. This work was performed in the G.L. and K.R.W. labs, which were supported by grants from the Robertson Investigator Award of the New York Stem Cell Foundation (to G.L.), the Maryland Stem Cell Research Fund (TEDCO) (to G.L. and K.R.W.), Muscular Dystrophy Association (to G.L.), FSH Society (to G.L.), and Team Saij (to G.L. and K.R.W.). T.V.H. is currently working at the NIH. This work was conducted while she was employed at the Kennedy Krieger Institute. The opinions expressed in this article are the author's own and do not reflect the view of the NIH, the Department of Health and Human Services, or the United States government.

Received: September 9, 2015
Revised: October 8, 2015
Accepted: April 30, 2016
Published May 26, 2016

REFERENCES

Arpke, R.W., Darabi, R., Mader, T.L., Zhang, Y., Toyama, A., Lonetree, C.L., Nash, N., Lowe, D.A., Perlingeiro, R.C., and Kyba, M. (2013). A new immuno-, dystrophin-deficient model, the NSG-mdx(4Cv) mouse, provides evidence for functional improvement following allogeneic satellite cell transplantation. Stem Cells *31*, 1611–1620.

Barberi, T., Bradbury, M., Dincer, Z., Panagiotakos, G., Socci, N.D., and Studer, L. (2007). Derivation of engraftable skeletal myoblasts from human embryonic stem cells. Nat. Med. *13*, 642–648.

Bennett, C.N., Ross, S.E., Longo, K.A., Bajnok, L., Hemati, N., Johnson, K.W., Harrison, S.D., and MacDougald, O.A. (2002). Regulation of Wnt signaling during adipogenesis. J. Biol. Chem. *277*, 30998–31004.

Bentzinger, C.F., Wang, Y.X., and Rudnicki, M.A. (2012). Building muscle: molecular regulation of myogenesis. Cold Spring Harb. Perspect. Biol. *4*, a008342.

Boldrin, L., Zammit, P.S., and Morgan, J.E. (2015). Satellite cells from dystrophic muscle retain regenerative capacity. Stem Cell Res. (Amst.) *14*, 20–29.

Borchin, B., Chen, J., and Barberi, T. (2013). Derivation and FACS-mediated purification of PAX3+/PAX7+ skeletal muscle precursors from human pluripotent stem cells. Stem Cell Reports *1*, 620–631.

Borowiak, M., Maehr, R., Chen, S., Chen, A.E., Tang, W., Fox, J.L., Schreiber, S.L., and Melton, D.A. (2009). Small molecules efficiently direct endodermal differentiation of mouse and human embryonic stem cells. Cell Stem Cell *4*, 348–358.

Brennand, K.J., Simone, A., Jou, J., Gelboin-Burkhart, C., Tran, N., Sangar, S., Li, Y., Mu, Y., Chen, G., Yu, D., et al. (2011). Modelling schizophrenia using human induced pluripotent stem cells. Nature *473*, 221–225.

Burridge, P.W., Matsa, E., Shukla, P., Lin, Z.C., Churko, J.M., Ebert, A.D., Lan, F., Diecke, S., Huber, B., Mordwinkin, N.M., et al. (2014). Chemically defined generation of human cardiomyocytes. Nat. Methods *11*, 855–860.

Cesana, M., Cacchiarelli, D., Legnini, I., Santini, T., Sthandier, O., Chinappi, M., Tramontano, A., and Bozzoni, I. (2011). A long noncoding RNA controls muscle differentiation by functioning as a competing endogenous RNA. Cell *147*, 358–369.

Chal, J., Oginuma, M., Al Tanoury, Z., Gobert, B., Sumara, O., Hick, A., Bousson, F., Zidouni, Y., Mursch, C., Moncuquet, P., et al. (2015). Differentiation of pluripotent stem cells to muscle fiber to model Duchenne muscular dystrophy. Nat. Biotechnol. *33*, 962–969.

Chambers, S.M., Fasano, C.A., Papapetrou, E.P., Tomishima, M., Sadelain, M., and Studer, L. (2009). Highly efficient neural conversion of human ES and iPS cells by dual inhibition of SMAD signaling. Nat. Biotechnol. *27*, 275–280.

Chen, H., Qian, K., Du, Z., Cao, J., Petersen, A., Liu, H., Blackbourn, L.W., 4th, Huang, C.L., Errigo, A., Yin, Y., et al. (2014). Modeling ALS with iPSCs reveals that mutant SOD1 misregulates neurofilament balance in motor neurons. Cell Stem Cell *14*, 796–809.

Darabi, R., Arpke, R.W., Irion, S., Dimos, J.T., Grskovic, M., Kyba, M., and Perlingeiro, R.C. (2012). Human ES- and iPS-derived myogenic progenitors restore DYSTROPHIN and improve contractility upon transplantation in dystrophic mice. Cell Stem Cell *10*, 610–619.

de Boer, A.S., Koszka, K., Kiskinis, E., Suzuki, N., Davis-Dusenbery, B.N., and Eggan, K. (2014). Genetic validation of a therapeutic target in a mouse model of ALS. Sci. Transl. Med. *6*, 248ra104.

Dequéant, M.L., and Pourquié, O. (2008). Segmental patterning of the vertebrate embryonic axis. Nat. Rev. Genet. *9*, 370–382.

Di Giorgio, F.P., Boulting, G.L., Bobrowicz, S., and Eggan, K.C. (2008). Human embryonic stem cell-derived motor neurons are sensitive to the toxic effect of glial cells carrying an ALS-causing mutation. Cell Stem Cell *3*, 637–648.

Dovey, H.F., John, V., Anderson, J.P., Chen, L.Z., de Saint Andrieu, P., Fang, L.Y., Freedman, S.B., Folmer, B., Goldbach, E., Holsztynska, E.J., et al. (2001). Functional gamma-secretase inhibitors reduce beta-amyloid peptide levels in brain. J. Neurochem. *76*, 173–181.

Dumont, N.A., Wang, Y.X., von Maltzahn, J., Pasut, A., Bentzinger, C.F., Brun, C.E., and Rudnicki, M.A. (2015). Dystrophin expression in muscle stem cells regulates their polarity and asymmetric division. Nat. Med. *21*, 1455–1463.

Fan, Y., Maley, M., Beilharz, M., and Grounds, M. (1996). Rapid death of injected myoblasts in myoblast transfer therapy. Muscle Nerve *19*, 853–860.

Fior, R., Maxwell, A.A., Ma, T.P., Vezzaro, A., Moens, C.B., Amacher, S.L., Lewis, J., and Saúde, L. (2012). The differentiation and movement of presomitic mesoderm progenitor cells are controlled by Mesogenin 1. Development *139*, 4656–4665.

Gussoni, E., Pavlath, G.K., Lanctot, A.M., Sharma, K.R., Miller, R.G., Steinman, L., and Blau, H.M. (1992). Normal dystrophin transcripts detected in Duchenne muscular dystrophy patients after myoblast transplantation. Nature *356*, 435–438.

Gussoni, E., Blau, H.M., and Kunkel, L.M. (1997). The fate of individual myoblasts after transplantation into muscles of DMD patients. Nat. Med. *3*, 970–977.

Hartel, J.V., Granchelli, J.A., Hudecki, M.S., Pollina, C.M., and Gosselin, L.E. (2001). Impact of prednisone on TGF-beta1 and collagen in diaphragm muscle from mdx mice. Muscle Nerve *24*, 428–432.

Hoffman, E.P., Brown, R.H., Jr., and Kunkel, L.M. (1987). Dystrophin: the protein product of the Duchenne muscular dystrophy locus. Cell *51*, 919–928.

Jasmin, G., Tautu, C., Vanasse, M., Brochu, P., and Simoneau, R. (1984). Impaired muscle differentiation in explant cultures of Duchenne muscular dystrophy. Lab. Invest. *50*, 197–207.

Karpati, G., Ajdukovic, D., Arnold, D., Gledhill, R.B., Guttmann, R., Holland, P., Koch, P.A., Shoubridge, E., Spence, D., Vanasse, M., et al. (1993). Myoblast transfer in Duchenne muscular dystrophy. Ann. Neurol. *34*, 8–17.

Kazuki, Y., Hiratsuka, M., Takiguchi, M., Osaki, M., Kajitani, N., Hoshiya, H., Hiramatsu, K., Yoshino, T., Kazuki, K., Ishihara, C., et al. (2010). Complete genetic correction of ips cells from Duchenne muscular dystrophy. Mol. Ther. *18*, 386–393.

Kiskinis, E., Sandoe, J., Williams, L.A., Boulting, G.L., Moccia, R., Wainger, B.J., Han, S., Peng, T., Thams, S., Mikkilineni, S., et al. (2014). Pathways disrupted in human ALS motor neurons identified through genetic correction of mutant SOD1. Cell Stem Cell *14*, 781–795.

Kornegay, J.N., Childers, M.K., Bogan, D.J., Bogan, J.R., Nghiem, P., Wang, J., Fan, Z., Howard, J.F., Jr., Schatzberg, S.J., Dow, J.L., et al. (2012). The paradox of muscle hypertrophy in muscular dystrophy. Phys. Med. Rehabil. Clin. N. Am. *23*, 149–172, xii.

L'Honoré, A., Coulon, V., Marcil, A., Lebel, M., Lafrance-Vanasse, J., Gage, P., Camper, S., and Drouin, J. (2007). Sequential expression and redundancy of Pitx2 and Pitx3 genes during muscle development. Dev. Biol. *307*, 421–433.

Li, H.L., Fujimoto, N., Sasakawa, N., Shirai, S., Ohkame, T., Sakuma, T., Tanaka, M., Amano, N., Watanabe, A., Sakurai, H., et al. (2015). Precise correction of the dystrophin gene in duchenne muscular dystrophy patient induced pluripotent stem cells by TALEN and CRISPR-Cas9. Stem Cell Reports *4*, 143–154.

Mali, P., Yang, L., Esvelt, K.M., Aach, J., Guell, M., DiCarlo, J.E., Norville, J.E., and Church, G.M. (2013). RNA-guided human genome engineering via Cas9. Science *339*, 823–826.

Martin, J.F., Schwarz, J.J., and Olson, E.N. (1993). Myocyte enhancer factor (MEF) 2C: a tissue-restricted member of the MEF-2 family of transcription factors. Proc. Natl. Acad. Sci. USA *90*, 5282–5286.

Mayeuf-Louchart, A., Lagha, M., Danckaert, A., Rocancourt, D., Relaix, F., Vincent, S.D., and Buckingham, M. (2014). Notch regulation of myogenic versus endothelial fates of cells that migrate from the somite to the limb. Proc. Natl. Acad. Sci. USA *111*, 8844–8849.

Mendell, J.R., Kissel, J.T., Amato, A.A., King, W., Signore, L., Prior, T.W., Sahenk, Z., Benson, S., McAndrew, P.E., Rice, R., et al. (1995). Myoblast transfer in the treatment of Duchenne's muscular dystrophy. N. Engl. J. Med. *333*, 832–838.

Millay, D.P., O'Rourke, J.R., Sutherland, L.B., Bezprozvannaya, S., Shelton, J.M., Bassel-Duby, R., and Olson, E.N. (2013). Myomaker is a membrane activator of myoblast fusion and muscle formation. Nature *499*, 301–305.

Mourikis, P., Gopalakrishnan, S., Sambasivan, R., and Tajbakhsh, S. (2012). Cell-autonomous Notch activity maintains the temporal specification potential of skeletal muscle stem cells. Development *139*, 4536–4548.

Ng, R., Banks, G.B., Hall, J.K., Muir, L.A., Ramos, J.N., Wicki, J., Odom, G.L., Konieczny, P., Seto, J., Chamberlain, J.R., and Chamberlain, J.S. (2012). Animal models of muscular dystrophy. Prog. Mol. Biol. Transl. Sci. *105*, 83–111.

Partridge, T.A. (2013). The mdx mouse model as a surrogate for Duchenne muscular dystrophy. FEBS J. *280*, 4177–4186.

Partridge, T.A., Morgan, J.E., Coulton, G.R., Hoffman, E.P., and Kunkel, L.M. (1989). Conversion of mdx myofibres from dystrophin-negative to -positive by injection of normal myoblasts. Nature *337*, 176–179.

Pegoraro, E., Hoffman, E.P., Piva, L., Gavassini, B.F., Cagnin, S., Ermani, M., Bello, L., Soraru, G., Pacchioni, B., Bonifati, M.D., et al.; Cooperative International Neuromuscular Research Group (2011). SPP1 genotype is a determinant of disease severity in Duchenne muscular dystrophy. Neurology *76*, 219–226.

Porter, J.D., Khanna, S., Kaminski, H.J., Rao, J.S., Merriam, A.P., Richmonds, C.R., Leahy, P., Li, J., Guo, W., and Andrade, F.H. (2002). A chronic inflammatory response dominates the skeletal muscle molecular signature in dystrophin-deficient mdx mice. Hum. Mol. Genet. *11*, 263–272.

Scott, J.M., Li, S., Harper, S.Q., Welikson, R., Bourque, D., DelloRusso, C., Hauschka, S.D., and Chamberlain, J.S. (2002). Viral vectors for gene transfer of micro-, mini-, or full-length dystrophin. Neuromuscul. Disord. *12* (*Suppl 1*), S23–S29.

Shelton, M., Metz, J., Liu, J., Carpenedo, R.L., Demers, S.P., Stanford, W.L., and Skerjanc, I.S. (2014). Derivation and expansion of PAX7-positive muscle progenitors from human and mouse embryonic stem cells. Stem Cell Reports *3*, 516–529.

Skuk, D., Goulet, M., Roy, B., Piette, V., Côté, C.H., Chapdelaine, P., Hogrel, J.Y., Paradis, M., Bouchard, J.P., Sylvain, M., et al. (2007). First test of a "high-density injection" protocol for myogenic cell transplantation throughout large volumes of muscles in a Duchenne muscular dystrophy patient: eighteen months follow-up. Neuromuscul. Disord. *17*, 38–46.

Tedesco, F.S., Gerli, M.F., Perani, L., Benedetti, S., Ungaro, F., Cassano, M., Antonini, S., Tagliafico, E., Artusi, V., Longa, E., et al. (2012). Transplantation of genetically corrected human iPSC-derived progenitors in mice with limb-girdle muscular dystrophy. Sci. Transl. Med. *4*, 140ra89.

Vo, A.H., and McNally, E.M. (2015). Modifier genes and their effect on Duchenne muscular dystrophy. Curr. Opin. Neurol. *28*, 528–534.

Wainger, B.J., Kiskinis, E., Mellin, C., Wiskow, O., Han, S.S., Sandoe, J., Perez, N.P., Williams, L.A., Lee, S., Boulting, G., et al. (2014). Intrinsic membrane hyperexcitability of amyotrophic lateral sclerosis patient-derived motor neurons. Cell Rep. *7*, 1–11.

Wang, K., McClure, J., and Tu, A. (1979). Titin: major myofibrillar components of striated muscle. Proc. Natl. Acad. Sci. USA *76*, 3698–3702.

Wang, J., Li, S., Chen, Y., and Ding, X. (2007). Wnt/beta-catenin signaling controls Mespo expression to regulate segmentation during Xenopus somitogenesis. Dev. Biol. *304*, 836–847.

Webster, C., Pavlath, G.K., Parks, D.R., Walsh, F.S., and Blau, H.M. (1988). Isolation of human myoblasts with the fluorescence-activated cell sorter. Exp. Cell Res. *174*, 252–265.

Wohlgemuth, S.L., Crawford, B.D., and Pilgrim, D.B. (2007). The myosin co-chaperone UNC-45 is required for skeletal and cardiac muscle function in zebrafish. Dev. Biol. *303*, 483–492.

Xu, C., Tabebordbar, M., Iovino, S., Ciarlo, C., Liu, J., Castiglioni, A., Price, E., Liu, M., Barton, E.R., Kahn, C.R., et al. (2013). A zebrafish embryo culture system defines factors that promote vertebrate myogenesis across species. Cell *155*, 909–921.

Zatz, M., Pavanello, R.C., Lazar, M., Yamamoto, G.L., Lourenço, N.C., Cerqueira, A., Nogueira, L., and Vainzof, M. (2014). Milder course in Duchenne patients with nonsense mutations and no muscle dystrophin. Neuromuscul. Disord. *24*, 986–989.